Available online at www.sciencedirect.com
ScienceDirect
Sensors and Actuators A 138 (2007) 269–275
SENSORS AND ACTUATORS A PHYSICAL
www.elsevier.com/locate/sna

Integrated micro-displacement sensor that measures tilting angle and linear movement of an external mirror

Itaru Ishikawa [a,*], Renshi Sawada [a,*], Eiji Higurashi [b], Shingo Sanada [a], Daisuke Chino [a]

[a] Department of Intelligent Machinery and Systems, Kyushu University, 744 Motooka, Nishi-ku, Fukuoka 819-0395, Japan
[b] Research Center for Advanced Science and Technology, University of Tokyo, 4-6-1 Komaba, Meguro-ku, Tokyo 153-8904, Japan

Received 16 November 2006; accepted 28 March 2007
Available online 6 April 2007

Abstract

An integrated optical micro-displacement sensor was developed that uses the beam diverging from a vertical cavity surface emitting laser (VCSEL). The sensor consists of a VCSEL (1.5 mm × 1.5 mm × 1.2 mm) that is surrounded by three photodiodes and can measure the linear distance traveled and the tilting angle of an external mirror. The resolution is 20 nm for a measurement range up to 0.4 mm, or less than 40 nm for a wider measurement range of 1.8 mm. The full range of the measurable tilting angle is 5°. This sensor can be incorporated into devices with micro-mirrors, such as integrated scanning microscopes.
© 2007 Elsevier B.V. All rights reserved.

Keywords: Optical lever; Measuring instrument; Displacement and rotation detection; VCSEL; MEMS

1. Introduction

Since the invention of the laser in 1960, optical measurement technology has developed remarkably. The invention of the semiconductor laser in 1970 activated research and development on compact measuring instruments, resulting in the commercialization of measuring instruments incorporating semiconductor lasers in 1980. The large and expensive conventional measuring instruments of yesterday have been transformed into portable units with the same functions and performance. And these measuring instruments are rapidly developing toward higher accuracy and functions, and at lower cost in the fields of robotics, household appliances, biotechnologies, communications, safety management, and environment analysis.

To utilize maximally the features of optical micro-machines for such purposes, optimal control and sensors for that control are essential. For example, micro-displacement sensors are required for the high-accuracy measurement of rotation angle and translational displacement using measuring instruments incorporating a Michelson's interferometer or a moving diffraction grating and high-accuracy positioning of optical elements. The development of MEMS is being accelerated by the addition of such measurement and control functions. Data recording using a vibrator sensor and proximity field light has been advancing steadily although some issues remain to be resolved.

Various types of displacement sensors based on triangulation or photo-interference have been developed. Integrated sensors fabricated using MEMS technologies have already been reported [1]. The structure of such first-generation sensors consisted of a polyimide waveguide formed on a laser diode with photodiodes monolithically integrated onto a gallium arsenide or silicon substrate. These sensors are very useful, but packaging difficulties have jeopardized their potential miniaturization and low cost, although there is no problem when they are incorporated directly inside a micro-machine. Another weakness is that the measuring distance is too short [2,3] to measure the tilt or displacement of a micromirror, as shown in Table 1.

Geometry-based measuring methods such as triangulation, optical beam deflection method (OBDM), and optical levers have such advantages as not requiring a reference optical beam, simple construction, and high sensitivity [4,5]. Simple construction enables dramatic miniaturization. Photo-divergence type displacement sensors are built so that the optical beams from the light source diverge at a specific angle. The farther an object is from a light source, the weaker the light reflected from the

* Corresponding authors. Tel.: +81 92 802 3241; fax: +81 92 802 3241.
E-mail addresses: itaru@nano-micro.mech.kyushu-u.ac.jp (I. Ishikawa), sawada@mech.kyushu-u.ac.jp (R. Sawada).

0924-4247/$ – see front matter © 2007 Elsevier B.V. All rights reserved.
doi:10.1016/j.sna.2007.03.027

Table 1
Measuring limit of previously reported sensor [1]

Type	Resolution (nm)	Measurable range
Long working distance	100	(Distance from the sensor: 80 μm) ±10 μm
Short working distance	9	(Distance from the sensor: 10 μm) ±5 μm

object. Thus, the displacement of optical beams in the direction of irradiation is measured using the fact that the intensity of the optical beams reflected from an object varies according to the displacement of the object. Although simple in construction, measuring instruments of this type feature high resolution, and some commercially available models even have resolutions of sub-nm order. Also many of these instruments, known as optical fiber displacement gauges, use optical fiber probes. This paper discusses displacement sensors that are based on the geometrical relationship between the incident and outgoing beam (often called an optical lever) and built using micro-machining technology. Sensors of this type, built in a mini *X*–*Y*–*Z* stage or micro-mirror, are very effective for measuring displacements in three axes (*X*, *Y*, *Z*) and rotation angles.

2. Measurement principle

Fig. 1 shows a conceptual diagram of the sensor we developed that measures the tilting angle or linear distance traveled of an external mirror. In this figure, a divergent light beam is emitted by a VCSEL toward the external mirror. The beam is incident to the sensor after reflection at the mirror. Tilting the mirror changes the shape of the reflected beam and linear displacement changes the size of the beam. The intensity of the light reaching two photodiodes (PD-A, PD-B) set on each side of the VCSEL thus changes in response to the tilt or linear displacement.

Fig. 2 shows the principle of linear displacement measurement using this sensor. The graph in the figure shows the schematic output characteristics of the signal, and the optical power received by the photodiode is plotted against the displacement of the mirror. The principle of linear displacement measurement using this sensor is the same as that of conventional beam divergence displacement sensors, and a peak for a specific displacement in the output characteristics is a feature of sensors of this type [4,6–8]. On the right-hand side of the peak (back slope), where the displacement is relatively large, the received light power decreases as the displacement increases. This occurs

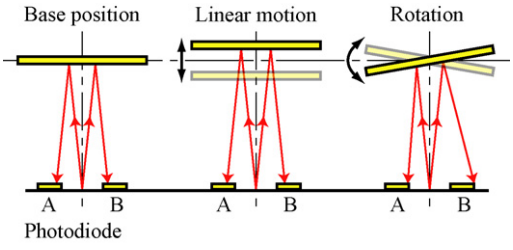

Fig. 1. Measurement principle of the new sensor.

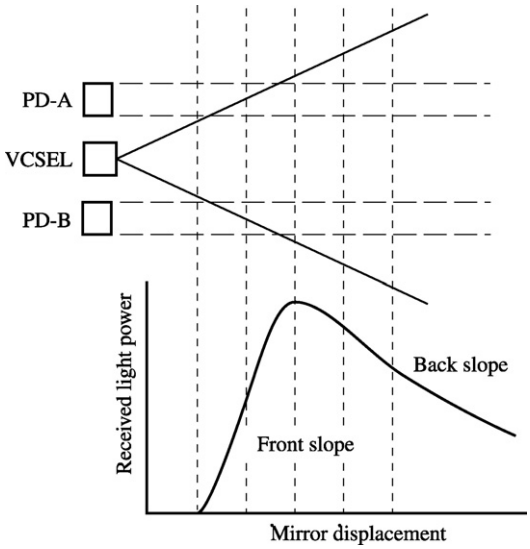

Fig. 2. Measurement principle of the displacement detection.

because the light beam diverges and the power of the reflected light decreases as the displacement increases. Conversely, on the left-hand side of the peak (front slope), where the displacement is relatively small, the received light power decreases as the displacement decreases. This occurs because the centers of the light source and the photodetector diverge from each other and the light does not enter the photodetector when the light source and photodetector are too close to the object, in which case the light divergence is insufficient and the photodetector is out of the range of the light reflected area. The displacement is measured using the linear part of the front and back slopes. The front slope is steep and used for a relatively precise measurement. The back slope is gradual and used for long-distance measurement. The sensor we developed has two photodiodes (PD-A and PD-B) and we used the sum of their outputs as the output of the displacement sensor. Thus, the output signal of the displacement measurement (S_{disp}) is a signal equivalent to:

$$S_{\mathrm{disp}} \equiv P_{\mathrm{A}} + P_{\mathrm{B}} \tag{1}$$

where P_{A} and P_{B} are optical powers received by PD-A and by PD-B, respectively.

The principle of the rotation angle measurement is based on the difference of the optical powers detected by the right and left PDs. That is, at the base position in Fig. 1, the intensities of the lights detected by the right and left PDs should be equal. When the mirror tilts toward a PD, the center axis of the light beam will move toward that PD. At a point closer to the center axis, the intensity of the light beam is higher, resulting in the difference between the intensities measured with the right and left PDs. The sensors we developed standardize the difference between the output signals of PD-A and PD-B with the sum of the signals and obtain the displacement angle S_{rot}.

$$S_{\mathrm{rot}} \equiv \frac{P_{\mathrm{B}} - P_{\mathrm{A}}}{P_{\mathrm{B}} + P_{\mathrm{A}}} \tag{2}$$

Thus, the output signal is equivalent to S_{rot}. The output signal versus tilt angle is given by a graph of the S-shaped curve shown

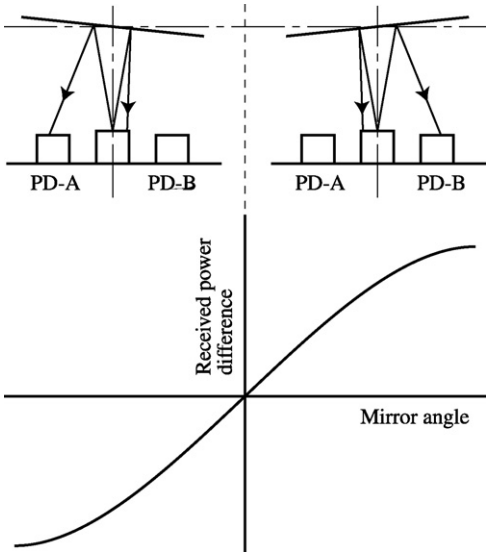

Fig. 3. Measurement principle of the angle detection.

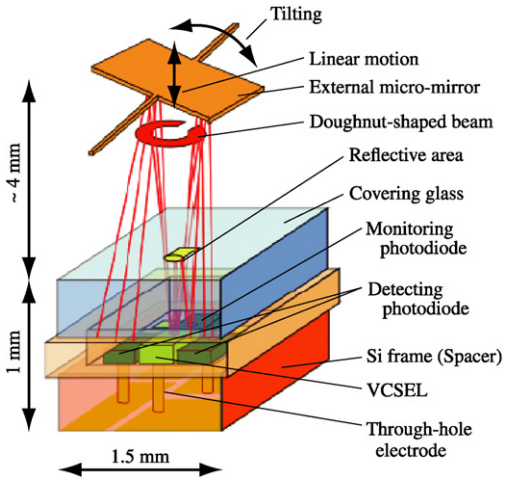

Fig. 4. Schematic of the new sensor's structure.

in Fig. 3. The angle is detected at the nearly linear part close to the center.

3. Fabrication and structure

Fig. 4 is a schematic drawing of the structure of the sensor we built. It is only 1.5 mm × 1.5 mm × 1.2 mm. The sensor consists of a cover glass, Si frame, and Si base substrate. A convex-shaped polyimide surface coated with a reflective Au film is formed on the top surface of the cover glass. The curvature of this surface directs the light beam that emerges from the very center of the VCSEL ($\lambda = 850$ nm, with a typical output power of 3.3 mW) to a monitoring photodiode after being reflected there, and this prevents the beam from returning to the VCSEL after being reflected at the mirror. Since the emitted light beam is blocked by the reflective convex surface, light emerging from the sensor's external mirror forms a doughnut-shape (strictly speaking, a "C" shape). The remaining reflective area functions as shading for the beam heading towards the monitoring photodiode after being reflected at the tilting or traveling mirror. The Si frame functions as a spacer, forming a gap between the cover glass and the silicon base substrate. The cover glass is also used as a sealing component.

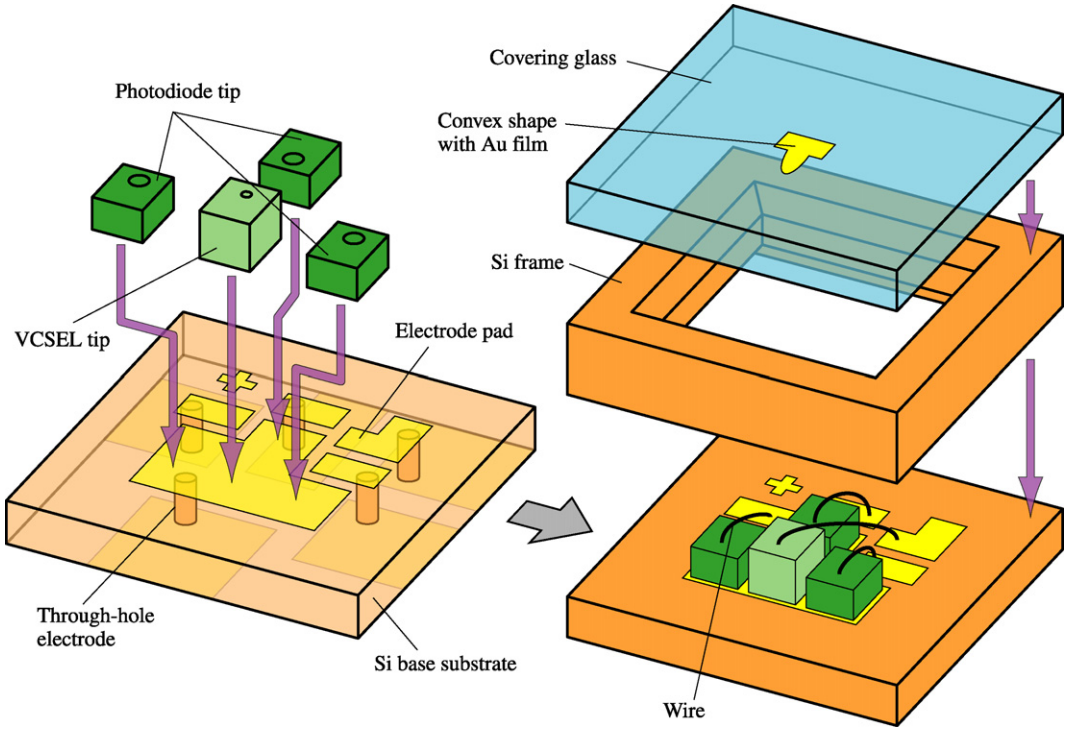

Fig. 5. Fabrication procedure.

Fig. 5 shows our sensor fabrication procedure. Optical components such as the VCSEL, the three photodiodes and wires connecting the components to the electrode pads are placed within the gap. The bottom is the silicon base substrate, with five through-hole electrodes to which the optical chips were bonded using patterned AuSn solder. Packaged sensors are formed by bonding these three components together. The Si frame and glass cover are bonded by anodic bonding [9], and the Si frame and base substrate are bonded by AgSn soldering.

Fig. 6 shows photographs of our fabricated sensor, with a cover glass with a reflective convex surface and shading bonded onto a Si frame and the Si base substrate.

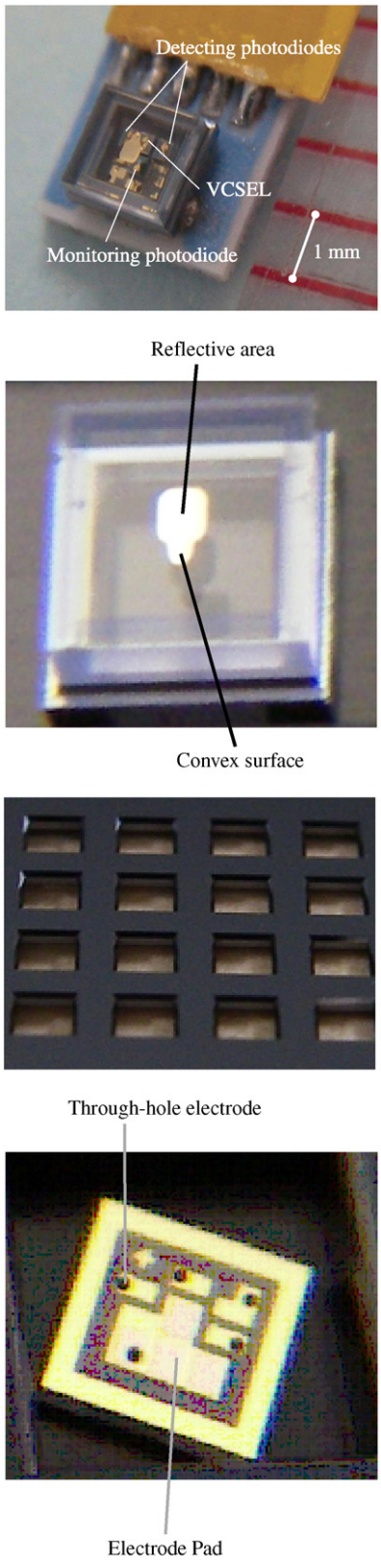

Fig. 6. (a) Fabricated packaged sensor. (b) Cover glass bonded onto the Si frame and reflective area. (c) Si frame substrate which is diced into pieces after having been bonded onto a cover glass. (d) Si base substrate for placement of the VCSEL and photodiodes.

4. Theoretical analysis

Before performing experiments and measurements, we calculated and simulated the sensor characteristics using the model shown in Fig. 7 and estimated the sensor output against the mirror movement. For simplicity, the covering glass is omitted in this model. In Fig. 7, a divergent Gaussian beam is emitted by the VCSEL. After being reflected by the external mirror, the beam is received by the detecting photodiodes (PD-A and PD-B), and this makes up the basic configuration of the sensor. The central clearance between the VCSEL and the detecting photodiode is 'l'. The photodiode's surface is located at lower position than that of the VCSEL by 'h'. The external mirror is placed at a distance 'd' from the VCSEL, and rotated at an angle 'θ'. When the mirror is parallel to the sensor, θ is zero. If the mirror were able to reflect the beam ideally, the reflected beam should seem to come from point A in Fig. 7, which is the image of the exit aperture of the VCSEL. The x–y–z orthogonal coordinate system that originates point A and x'– y' coordinate system which lies on the plane of the photodiodes is set as shown in Fig. 7. From the geometry in Fig. 7, $s = (d + h)/\cos(2\theta)$ and $t = (d + h)\tan(2\theta)$ are defined.

The objective of this analysis is to derive the relationship between the incident power into the detecting region of the photodiodes and the mirror position (d, θ). The incident power can be defined by integrating the irradiance on the area of the detecting region. We therefore first derive the irradiance on the plane of the photodiodes (x'– y' plane). After that, the irradiance is integrated on the area of the detection regions of the photodiodes to obtain the incident power.

If this beam waist is placed on the face of the VCSEL, the transverse irradiance of the Gaussian beam that emerges from point A is given by

$$I(x, y, z) = \frac{2P}{\pi w(z)^2} \exp\left(-\frac{2(x^2 + y^2)}{w(z)^2}\right) \quad (3)$$

where P is the optical power and $w(z)$ is the beam half-width. If the beam diverges with the full-angular width of Θ, the beam half-width w varies according to

$$w(z) = z \tan(\Theta/2) \quad (4)$$

provided z is much larger than the beam waist.

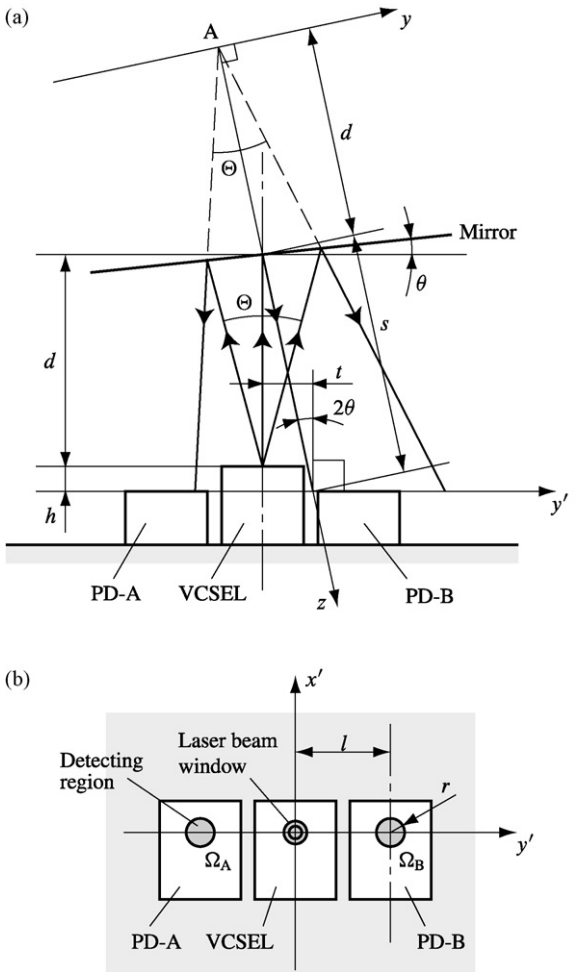

Fig. 7. Analysis model of the new sensor: (a) front view and (b) top view.

The plane of the photodiodes is expressed in the x–y–z coordinate system as follows

$$z = y\ \tan(2\theta) + (d + s) \tag{5}$$

The function I_{PD} expresses the function obtained by substituting this equation for Eq. (3).

$$I_{PD}(x, y) = I(x, y, z)|_{z \to y\ \tan(2\Theta)+(d+s)} \tag{6}$$

where $I(x, y, z)|_{z \to y\ \tan(2\Theta)+(d+s)}$ means that the variable z in $I(x, y, z)$ is replaced by $y\ \tan(2\Theta) + (d + s)$. An expression like this will be used in the following derivation to avoid redundant descriptions and to clarify the elicitation process. The function $I_{PD}(x, y)$ represents the irradiance of the beam that directs the z direction on the x'– y' plane. The irradiance ingredient $I'_{xy}(x, y)$ that passes the x'– y' plane perpendicularly is found by multiplying $\cos(2\theta)$ by $I_{PD}(x, y)$.

$$I'_{xy}(x, y) = \cos(2\theta) \times I_{PD}(x, y) \tag{7}$$

Additionally, $x \to x'$ and $y \to (y' - t)\ \cos(2\theta)$ are performed to replace the variables (x, y) with (x', y').

$$I'(x', y') = I'_{xy}(x, y)|_{(x \to x', y' \to (y'-t)\ \cos(2\theta))} \tag{8}$$

The function $I'(x', y')$ represents the irradiance that passes through the x'– y' plane perpendicularly, after all of the above manipulations are carried out in sequence, finally the irradiance $I'(x', y')$ is expressed as follows

$$I'(x', y') = I'_0\ \exp\left(-\frac{2x'^2}{w'^2}\right)\ \exp\left(-\frac{2y''^2}{w'^2}\right) \tag{9}$$

where

$$I'_0 = \frac{2P\ \cos(2\theta)}{\pi w'^2} \tag{10}$$

$$w' = (y'\ \sin(2\theta) + d_c)\ \tan(\Theta/2) \tag{11}$$

$$y'' = y'\ \cos(2\theta) - d_s \tag{12}$$

$$d_c = (d + h)\ \cos(2\theta) + d \tag{13}$$

$$d_s = (d + h)\ \sin(2\theta) \tag{14}$$

By integrating $I'(x', y')$ on the area of the detecting regions of the photodiodes, we estimated the power received by the photodiodes. The area of the detecting region of PD-A 'Ω_A' and of PD-B 'Ω_B' is defined below:

$$\Omega_A = \{(x', y')|x'^2 + (y' + l)^2 \le r^2\} \tag{15a}$$

$$\Omega_B = \{(x', y')|x'^2 + (y' - l)^2 \le r^2\} \tag{15b}$$

With the area on the x'– y' plane expressed by Ω, the optical powers received by the photodiodes are calculated using the following equation:

$$P_A = \int_{\Omega_A} I'(x', y')\, d\Omega \tag{16a}$$

$$P_B = \int_{\Omega_B} I'(x', y')\, d\Omega \tag{16b}$$

We calculated the integration in Eq. (16) using Mathematica software, and obtained the displacement signal S_{disp} and angle signal S_{rot} according to Eqs. (1) and (2). The parameters were set according to the actual sensor dimensions. Fig. 8 is a graph of the mirror displacement (d) and displacement signal S_{disp}. This is a characteristic sensor graph having a front slope, detected

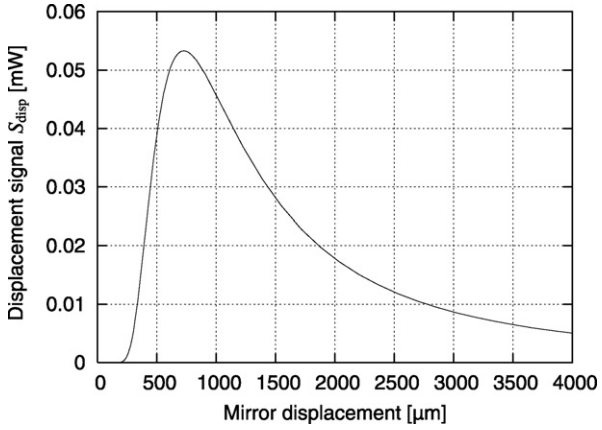

Fig. 8. Simulation result of the displacement signal.

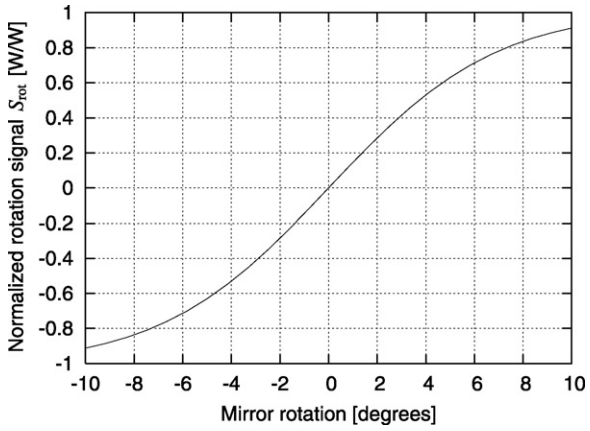

Fig. 9. Simulation result of the rotation signal.

power peak and back slope. In Fig. 9, the angle signal S_{rot} is plotted against the mirror rotation angle (θ). This graph shows a signal waveform of an S-shaped curve.

5. Experimental results

The actual relationship between the linear motion or tilt angle of the external mirror and the voltage output of the photodiodes is shown in Fig. 10. The axis of the ordinates is the outputs of the photodiodes amplified with an electronic circuit and then processed into S_{disp}, S_{rot} as defined by Eqs. (1) and (2). These graph are based on measurements made with sensors that had the covering glass and Si frame (spacer) removed. The reason for this configuration is that the front slope could not be obtained fully with sensors that had a covering glass because the thickness of the glass prevented the mirror from approaching VCSEL and PD sufficiently.

In the linear motion-output voltage curve, the linear region corresponds to the measurable range. Also, the measurement accuracy (resolution) was determined by the linearity of the displacement-output voltage curve and the output noise level of the sensor. The wider the range, the poorer the resolution. When the linearity is very high, the achievable measurement accuracy can be estimated roughly with NFWHM/ $\sin\alpha$, where

- NFWHM: full width at half maximum of the noise.
- α: tilt angle of the curve excluding noise ($= \tan^{-1}(\partial S_{disp}/\partial d)$).

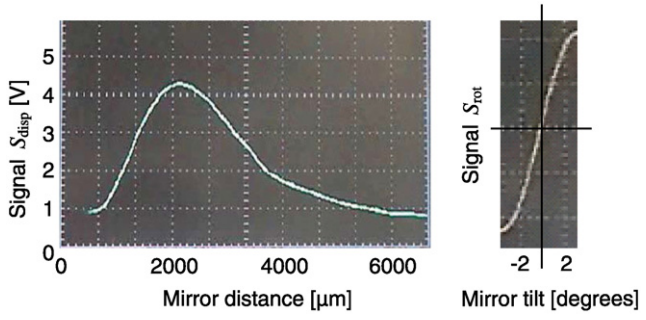

Fig. 10. Measured signal.

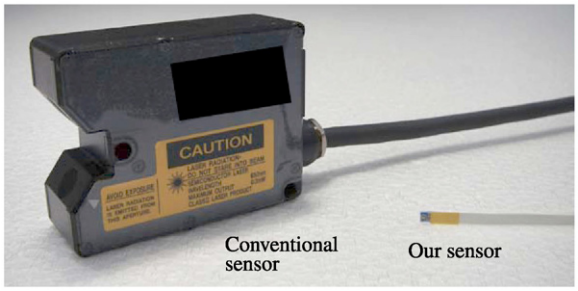

Fig. 11. Photograph comparing a commercially available conventional sensor (left) based on an optical lever and our new sensor (right).

In the vicinity of the sensor, the curve is linear with a larger gradient. High measurement accuracy can be obtained in the front slope because of the large "α". The smallest resolution obtainable in the front region was 20 nm up to a measurement range of 0.4 mm. In the back region, the resolution was less than 40 nm for a wider measuring range of 1.8 mm.

For the tilt-output plot, an S-shaped curve was obtained. The measurement range of our fabricated sensor is -2.5° to $+2.5^\circ$, giving a full range of 5°.

6. Discussion

Fig. 11 is a photograph of a commercially available conventional sensor and the sensor we fabricated and present in this paper. Clearly, MEMS technology has enabled the sensor to be dramatically miniaturized. Table 2 compares both types of sensors and shows that our newly developed sensor has measurement distance and accuracy comparable with conventional sensors.

A feature of our new sensor is that its measurable range can be optimized by forming a lens on the covering glass or by changing the distance between the detecting photodiodes and VCSEL. We could not utilize fully the front slope with high sensitivity when our new sensor was provided with a covering glass. A way to solve this problem is to form a lens on the covering glass and change the beam divergence angle.

The monolithically integrated sensor that we reported on previously [1] is smaller (0.8 mm × 0.75 mm) than the sensor we discussed in this paper, but it was difficult to reduce its cost due to packaging difficulties. But, the packaging costs for our new sensor can be reduced. By forming the photodiodes on the Si substrate, and molding a covering glass, the sensor can be made less expensive. Further, our new sensor is small enough to be incorporated in various types of micro-devices. Also, our new sensor has a resolution of 20 nm for a measuring distance of up to 0.4 mm, whereas the monolithically integrated sensor has a resolution of 9 nm for operating distances of 10 μm (Table 1).

Table 2
Measuring limit of conventional sensors and fabricated sensor

	Conventional sensor	Our sensor
Measuring range (mm)	2	1.8
Resolution (nm)	20	40

Our new sensor features a greatly improved measuring distance although it has a somewhat inferior resolution.

Compared to our simulation results, in our experimental measurements taken on a linear motor, the new sensor exhibited lower sensitivity and a different peak position. We think that these results were caused by the existence of the mirror rotation angle, difference in the bean divergence angle of VCSEL, alignment error of VCSEL or PD during bonding, or the shadow of the wiring. We also think that the slight difference in the mirror rotation between our experimental measured values and the results of our simulation was caused by the fact that the expected position "*d*" of the mirror was different from the measured value.

Our new sensor can detect the mirror rotation angle around one axis. By providing detecting photodiodes not only on the right and left sides of the VCSEL, but also over and under the VCSEL, a two-axis sensor unit can be easily configured.

7. Conclusions

A small (1.5 mm × 1.5 mm × 1.2 mm), high-resolution, packaged displacement sensor was developed that can measure the tilt angle or linear distance traveled of an external mirror. The smallest resolution obtained in the vicinity of the sensor is 20 nm for a measurement range of up to 0.4 mm. The full range of the measurable tilting angle is 5°. The measurement range and resolution can be adjusted by forming a lens on the covering glass or by changing the distance between the two detecting photodiodes. These capabilities for a one-axis micro-mirror can be expanded to use for a two-axis mirror.

Acknowledgements

This study was supported in part by the New Energy and Industrial Technology Development Organization (NEDO) of Japan. The authors also wish to thank Yoshinori Kimura and Atsushi Onoe of Pioneer Ltd. and Takeshi Kobayashi of AIST for fabricating the reflective regions of the cover glasses.

References

[1] T. Ito, R. Sawada, E. Higurashi, Integrated micro-displacement sensor that uses beam divergence, J. Micromech. Microeng. 13 (2003) 942–947.
[2] F. Lamarque, C. Prelle, P. Revel, Long range and nanometric resolution sensor for non-contact position measurement, in: Proceedings of the IEEE Sensors, vol. 3, 2004, pp. 1542–1545.
[3] C. Prelle, P. Lamarque, P. Revel, Reflective optical sensor for long-range and high-resolution displacements, Sens. Actuators A 127 (2006) 139–146.
[4] R.O. Cook, C.W. Hamm, Fiber optic lever displacement transducer, Appl. Opt. 18 (19) (1979) 3230–3241.
[5] E. Higurashi, R. Sawada, T. Ito, Monolithically integrated optical displacement sensor based on triangulation and optical beam deflection, Appl. Opt. 38 (9) (1999) 1746–1751.
[6] N. Ikawa, S. Shimada, H. Morooka, Photoelectronic displacement sensor with nanometre resolution, Precis. Eng. 9 (2) (1987) 79–82.
[7] D. Sagrario, P. Mead, Axial and angular displacement fiber-optic sensor, Appl. Opt. 37 (1998) 6748–6754.
[8] P.B. Buchade, A.D. Shaligram, Simulation and experimental studies of inclined two fiber displacement sensor, Sens. Actuators A 128 (2006) 312–316.
[9] H. Henmi, S. Shoji, Y. Shoji, K. Yoshimi, M. Esashi, Vacuum packaging for microsensors by glass-silicon anodic bonding, Sens. Actuators A 43 (1994) 243–248.